Materials Research. 2023; 26(suppl. 1):e20220599
DOI: https://doi.org/10.1590/1980-5373-MR-2022-0599

Optimization of Drilling Cuttings Reactivity as a Supplementary Cementitious Material in Ternary Cements

Kuelson Rândello Dantas Maciel[a,b]*, Ana Rita Damasceno Costa[c], Josinorma Silva de Oliveira[a], Heloysa Martins Carvalho Andrade[a], Jardel Pereira Gonçalves[a,c]

[a]*Universidade Federal da Bahia (UFBA), Centro Interdisciplinar de Energia e Ambiente (CIENAM), Salvador, BA, Brasil.*
[b]*Universidade Federal do Oeste da Bahia (UFOB), Centro das Ciências Exatas e das Tecnologias, Barreiras, BA, Brasil.*
[c]*Universidade Federal da Bahia (UFBA), Escola Politécnica, Pós-graduação em engenharia Civil (PPEC), Salvador, BA, Brasil.*

Received: December 17, 2022; Revised: May 05, 2023; Accepted: August 16, 2023

This study evaluates the influence of milling on the reactivity of drilling cuttings (DC) utilized as supplementary cementitious material in ternary cements (TC). The drilling cuttings milling study varied the time (2, 5, 10, 15, and 20 min) and rotation speed (200 and 300 rpm), determining the specific milling energy and grindability index. The hydration of TC pastes containing DC with different particle size distributions was evaluated by isothermal calorimetry during the first 72 hours, XRD/Rietveld at 3 and 28 days, compressive strength and absorption. The incorporation of milled DC improved the TC hydration kinetics compared to reference pastes of ordinary Portland cement (REF.PC). After 28 days, the TC pastes with the $D_{50\%}$ diameter smaller than 11 µm reached at least 70% of the resistance to the strength of the Portland cement paste. Milled DC contributes to the physical and nucleation effect of the TC pastes studied and can be used as an SCM.

Keywords: *Ternary cement, Supplementary cementitious materials, Drilling cuttings, Milling, Waste management.*

1. Introduction

Carbon dioxide emissions associated with cement production account for 8% of total global emissions, and it is estimated that cement consumption could quadruple by 2050, especially in developing countries[1,2]. In this sense, using cement made with locally available raw materials with low embodied energy would provide significant benefits for the sustainability of construction[3]. Using supplementary cementitious materials (SCM) with pozzolanic reactivity for partial clinker replacement is a promising solution[4-10]. Among the alternatives containing SCM, ternary cement (TC) or limestone calcined clay cement was developed. Replacing Portland cement by up to 50% with a combination of these materials provides a solution with reduced cost and energy, in addition to mechanical properties comparable to ordinary Portland cement[8,11,12].

Milling is a typical process in cement manufacturing. It has been used to reduce the particle size of natural materials or wastes for use as SCM, such as granulated blast furnace slag[13,14]. Several studies have explored increasing the reactivity of SCM through milling. Zunino and Scrivener[15] demonstrated that the milling of calcined clay followed by the air separation technique allows the isolation of the most reactive clay minerals in the fraction of smaller diameter and, therefore, the separation of inert compounds of larger particle size, such as quartz and iron oxide. Milling zeolites for up to 4 hours increases the filler effect and pozzolanic reactivity when incorporated into TC[16]. Although several studies have explored the increase in clay reactivity through milling, the influence of this beneficiation on the properties of Drilling cuttings (DC) for use as SCM remains unexplored.

One of the main residues from drilling oil and gas wells is DC, which consist of rock fragments with adhered drilling fluid and fragments of cured cement, depending on the drilling phase. Managing DC is a problem in the oil industry due to the large amounts generated and the presence of potentially contaminating substances such as polycyclic aromatic hydrocarbons, polychlorinated biphenyls and heavy metals (barium, lead, zinc, mercury, chromium, arsenic and nickel)[17]. The national production of drilling cuts and drilling fluids is estimated at approximately 14 thousand tons/year, a large part of which is directed to industrial landfills and recovery, recycling and reuse[18]. DC have been used to produce clinker[19,20], de concrete[21,22], mortar[23,24], paving materials[25,26] and ceramics[27,28].

The production of ternary cement (TC) types using residual raw materials has already been demonstrated[29-31]. The technique contributes to reducing CO_2 emissions, energy consumption and the extraction of natural raw materials[31-34]. The variability of binary additions of fly ash and limestone affect the physical and rheological properties of composite cement milled to provide an ideal ratio to produce TC[35].

*Corresponding author: kuelson.maciel@ufob.edu.br

Costa and Gonçalves[5] investigated TC carbonation using supercritical carbon dioxide ($ScCO_2$) as an alternative method to accelerate the process. TC types were produced from waste raw materials, including waste ceramic brick, ceramic tiles, marble and phosphogypsum. Using ceramic brick for replacing calcined clay in TC resulted in the highest amount of carbo aluminates among the investigated pastes, and high resistance to both axial compression and attack by $ScCO_2$. Cardoso et al.[36] demonstrated the feasibility of producing TC using different proportions of non-calcined kaolinitic clay, limestone and Portland clinker. Costa et al.[6] showed that TC containing cement, phosphogypsum and marble plus ceramic waste can be used sustainably as an alternative to natural raw materials for producing TC.

Marble waste is a by-product of marble processing. Worldwide marble production is estimated at 38 million tons per year[37]. The cutting and polishing process generates around 25% of residue in relation to the total mass of marble manufactured[38]. Its main mineral composition is calcium carbonate ($CaCO_3$) and dolomite ($MgCa(CO_3)_2$), with minor fractions of other minerals, such as quartz, feldspar, and mica[39].

Phosphogypsum (PG) is the calcium sulfate hydrate formed as a by-product of the production of fertilizer from phosphate rock. The high concentration of gypsum ($CaSO_4.2H_2O$) and bassanite ($CaSO_4.0{,}5H_2O$) allows it to be potentially added to the clinker to stabilize the setting time[40]. The world production of PG is estimated at approximately 160 million tons per year, currently, but it could reach up to 250 million tons in the next decade[41].

Currently, a growing number of studies show the potential use of TC as an alternative that causes less environmental impact compared to Portland cement. Although recent studies have been directed towards expanding the use of waste to replace natural raw materials[6,29], it appears that the effect of adding DC on the production of TC has not been studied yet. Given the high annual amounts generated from this waste[18], its application in TCs as an alternative to natural clay sources would have ample potential for reuse.

This study evaluates how milling affects the reactivity of DC applied as SCM in ternary cement. The raw materials used were Brazilian-type V ARI Portland cement as a clinker source, marble residue as an alternative to limestone, phosphogypsum as a substitute for gypsum, and DC as a substitute for non-calcined clay.

2. Materials and Methods

2.1. Materials

The DC samples originated from an onshore drilling rig in Candeias, Bahia, Brazil. The Bahia Beige type waste marble (WM) was obtained from a company that cuts and manufactures ornamental pieces in Salvador, Bahia, Brazil. The PG provided by a fertilizer industry in Uberaba, Minas Gerais, was collected manually from the stockpiles at different sampling points. Finally, to the reference set, the same amounts of both SCMs and quartz, as an inert material, were added to evaluate the filler effect contribution. High Initial Strength Type V Portland Cement (PC V ARI) was added to all mixtures. The choice of cement was based on local availability, high reactivity and smaller particle size. The physical properties of the raw materials are shown in Table 1.

The particle size distribution of Portland cement (PC), waste marble (WM) and phosphogypsum (PG) are shown in Figure 1.

The chemical composition of the raw materials (Table 2) was obtained using an X-ray fluorescence spectrometer (FRX) model S8 Tiger (Bruker). Loss on ignition (LOI) was determined by thermogravimetric analysis (TGA) using a DTG-60H thermal analyzer (Shimadzu). Approximately 10 mg of the powder samples were placed in an aluminum crucible and analyzed at temperatures varying from 25 to 1000 °C, 50 mL.min^{-1} N_2 flow and 10 °C.min^{-1} heating rate. The Portland cement (PC) used consists mainly of calcium and silicon oxides. DC consist predominantly of SiO_2, Al_2O_3 and Fe_2O_3. The presence of TiO_2 generally indicates the sedimentary origin[27]. DC showed a high LOI due to the decomposition of clay mineral contents and dehydroxylation of kaolinite between 400 and 570 °C. WM consisted mainly of $CaCO_3$ and exhibited high LOI due to decomposition (Equation 1) between 500 and 800 °C. Based on the molar masses of $CaCO_3$ and CO_2 (100.09 and 44.01 g/mol, respectively), it is observed that the mass loss due to carbonate decomposition is about 44%. Thus, the WM mass loss (41.49%) indicates a high $CaCO_3$ content. PG consists mainly of CaO and SO_3, consistent with its main phases, di-hydrated, hemi-hydrated and anhydrous calcium sulfates.

Table 1. Physical properties of raw materials.

Properties	PC	WM	PG
Specific gravity (kg m^{-3})	3272	2781	2438
Specific heat (J g^{-1} °C^{-1})	1.13	1.25	1.08
D_{10} (μm)	1.87	0.73	1.37
D_{50} (μm)	11.60	3.69	7.98
D_{90} (μm)	34.08	15.33	32.05

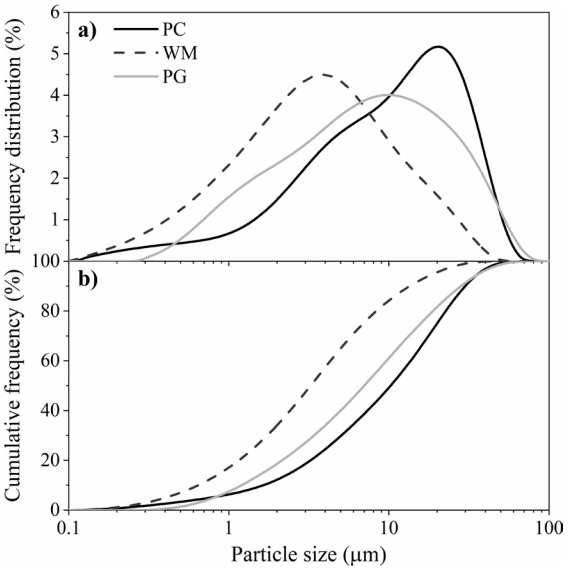

Figure 1. Particle size distribution of raw materials (a) frequency distribution and (b) cumulative frequency.

$$CaCO_3 \rightarrow CaO + CO_2 \quad (1)$$

The drilling cuttings were crushed in a Pavitest/Contenco model I-4198 jaw crusher (Figure 2). The smaller grain size fraction was then separated through a 1.18 mm aperture sieve aided by a mechanical stirrer for 15 min.

2.2. DC milling study

After sieving, the DC fractions with particles smaller than 1.18 mm were milled using a planetary ball mill model PM 100 (Retsch) equipped with a 500 cm^3 stainless steel jar. DC samples were oven-dried at 35 °C for 12 hours. For each milling, 1600 steel spheres with 5 mm diameter and 75 mL of sample were used, leaving one-third of the jar volume free, following the manufacturer's recommendations (Retsch). The sample volume was fixed, and the weight was calculated from the specific mass and determined as 2710 $kg.m^{-3}$ using a helium gas pycnometer, model AccuPyc II 1340. Therefore, a sample of 202.97 g was milled at a varying rotation speed (200 and 300 rpm) and times (2, 5, 10, 15, and 20 min).

Table 2. Chemical composition of raw materials (%).

Oxides	PC	DC	WM	PG
CaO	59.02	2.21	49.03	33.02
SiO_2	15.38	52.71	4.53	1.10
MgO	6.38	3.30	3.71	0.02
SO_3	4.92	0.16	0.04	40.43
Al_2O_3	3.33	18.59	0.45	0.11
Fe_2O_3	2.97	7.66	0.27	0.48
K_2O	0.91	2.85	0.07	<0.01
TiO_2	0.21	0.92	0.03	0.68
P_2O_5	0.11	0.16	0.01	0.73
Na_2O	0.10	1.23	-	-
SrO	0.07	0.02	0.02	0.56
Others	0.20	0.28	0.76	0.08
LOI*	6.40	9.91	41.49	22.34

*: Loss on ignition (1000 °C) determined by TGA.

Specific milling energy (SME) is defined as the energy consumed per unit of product and is used to define energy consumption (from oil, natural gas, and electricity) per ton of processed product (raw materials, clinker, cement). Generally, cement factories use electrical energy for milling the raw materials using ball mills. Therefore, the SME is expressed by Equation 2[42], where SME is the specific milling energy of the raw materials expressed in kWh/t of raw material.

$$SME = Energy\ consumption(kWh) / Mass\ of\ material\ milled(ton) \quad (2)$$

The grindability index[43] (GI) reflects the pulverizing potential of a material. This parameter is associated with the amount of new surface produced during milling and can be determined by the ratio between the specific surface area of the milled material and the energy consumed by the milling equipment[44]. The specific surface area of the drilling cuttings after each milling cycle was estimated based on the particle size distribution curve.

2.3. Particle size distribution by laser diffraction

The particle size distribution of the raw materials after each milling cycle was the parameter chosen and applied to the variables of the milling study. For this purpose, the particle size distribution was determined using a Mastersizer model 3000 laser diffraction equipment (Malvern Instruments) equipped with an Aero S accessory for dispersing dry powder of milled and non-milled DC.

2.4. Production and cure of cement pastes

To produce the types of ternary cement, 100 g of the raw materials were manually mixed by shaking the closed container for 60 seconds. A ternary cement with added DC and two reference compositions were produced.

The first was a pure Brazilian High Early Strength Portland cement (REF.PC), in the second (REF.Q), a quartz amount equal to the sum of the clay source (DC) and marble waste was added as inert material. However, since the Portland cement used already had 0.94% of anhydrite added to stabilize the setting time, a value correction was applied to maintain the content of the calcium sulfate phases at 5%. The composition of the cement pastes is shown in Table 3.

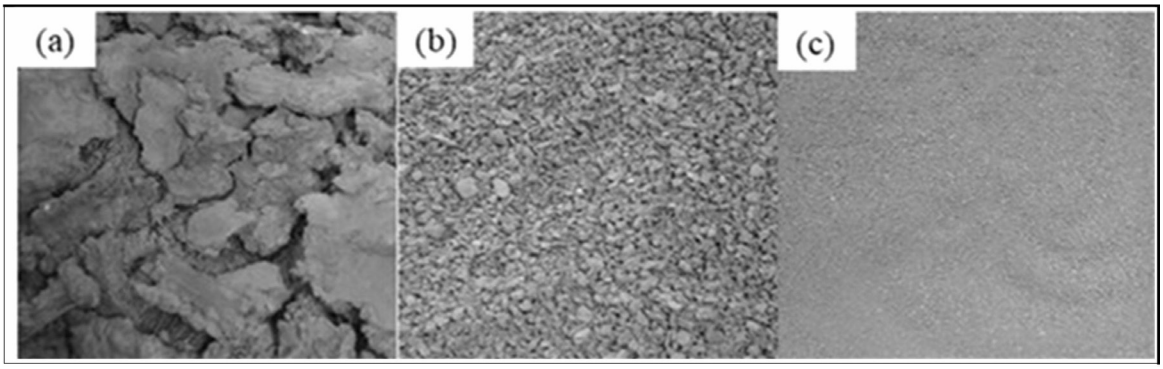

Figure 2. DC in natura (a), crushed (b) and sieved (c).

The water/cement ratio was set at 0.55 for all experimental analyses. The high ratio stems from the increased demand for water due to the high specific surface area of supplementary cementitious materials, mainly clays[45,46].

The mixing procedure was carried out in a Hamilton HMD 200 mixer (FANN), according to the following steps: a) add water; b) add anhydrous material already homogenized; c) mix for 2 min at 21000 rpm; d) 1 min pause for manual mixing, to loosen the material adhered to the container walls and break possible granules of dry material; e) mix at 14000 rpm for 2 min. The samples were demolded 24 hours later and submerged in curing water without additives at 20 °C and cured for 1, 3, and 28 days.

2.5. Isothermal calorimetry

The hydration kinetics of cementitious pastes with added DC of five different particle sizes was determined by isothermal calorimetry. The heat flow was evaluated during the first 72 hours of hydration at 20 °C. For this purpose, a TAM Air isothermal calorimeter (TA Instruments), with 20 μW precision and eight channels, was used to determine the cumulative heat and the differential heat of the pastes. In a plastic beaker, 100 g of binder and 55 g of deionized water were mixed at 12000 rpm for 2 minutes. Approximately 6 g of the sample was transferred into a 20 mL glass ampoule, which was sealed and then placed in the instrument.

The test was carried out in accordance with the standards ASTM C1679[47] e ASTM C1702[48]. Isothermal calorimetry was used to understand how the addition of milled DC affected cement hydration. The heat data were normalized considering the amount of Portland cement (OPC) included in the ternary cement.

Table 3. Composition of pastes (wt%).

Materials	REF.PC	REF.Q	TC
PC	100.00	50.85	50.85
DC	0.00	0.00	30.00
WM	0.00	0.00	15.00
Q	0.00	45.00	0.00
PG	0.00	4.15	4.15
Water/solids	0.55	0.55	0.55

2.6. X-ray diffractometry (XRD) and quantitative analysis by the Rietveld method

XRD was used to determine the mineralogical composition of raw materials and cement pastes. The D8 Advance (Bruker AXS) diffractometer settings were as follows: Cu Kα radiation (λ = 0.154 nm) at 21 °C with a 0.02^0 step per second, in a 5 to 80º range (2θ); the X-ray tube were operated at 40 kV and 40 mA. The crystalline phases in each diffractogram were interpreted from crystallographic sheets existing in the Inorganic Crystal Structure Database (ISCD) of the software Highscore plus 3.0.5. The phases were quantified using the software GSAS II[49], which uses the Rietveld method and CIF files (Crystallographic Information File) obtained from ICSD system. The general parameters of scale factor, background curve (Chebyshev polynomial), sample displacement, unit cells, and finally, the instrumental parameters of the peak shape (W, X, V, U and SH/L) were refined using the software GSAS II. The goodness of fit was evaluated by the chi-square factor (X^2), which corresponds to the Goodness of Fit (GOF). In GSAS II, X^2 is the sum of squared deviations between observed and calculated values for each data point. Generally, the result is considered reliable if X^2 lies in the 1.0 to 2.0 range[50].

The degree of crystallinity method was used to determine the content of amorphous and unquantified crystalline phases (ACn) in the samples. This approach consists of estimating the percentage of crystallinity by calculating the areas referring to crystalline (XRD peaks) and non-crystalline (below baseline) phases in a diffraction interval[51]. The ACn content was adjusted by a single peak obtained from the pseudo-Voigt function applied to the diffractogram baselines. The content of non-crystalline phases is given by the ratio of the areas associated with the ACn (the area under the pseudo-Voigt function) and the total area below the diffractogram[52].

3. Results and Discussion

3.1. DC milling study

The particle size distribution of drilling cuttings (DC) before and after milling is shown in Table 4 and Figure 3. The particle size (Table 4) indicates that milling in a planetary ball mill between 200 and 300 rpm for 2 to 20 min reduced particle size efficiently. Milling reduced the size of DC

Table 4. Physical properties of DC samples before and after milling.

Time (min)	Speed (rpm)	$D_{10\%}$ (μm)	$D_{50\%}$ (μm)	$D_{90\%}$ (μm)	Estimated specific surface area ($m^2\ kg^{-1}$)
0	0	150	2075.66	4581.20	-
2	200	6.53	272.31	1524.13	129.88
5		4.02	89.44	1056.83	215.66
10		2.27	18.89	253.50	371.69
15		1.91	12.65	230.67	453.65
20		1.73	10.22	146.60	492.88
2	300	2.88	27.95	304.50	298.82
5		1.60	8.58	81.97	632.11
10		1.60	8.55	80.70	633.24
15		1.52	8.54	81.87	701.11
20		1.40	7.64	86.06	774.91

particles (>100 μm) in natura and increased the fractions from 1 to 10 μm as indicated by the frequency curve shifting to the left (Figure 3). The particle size distribution was similar for milling at 300 rpm and the milling times of 10, 15 and 20 min (Figure 3). According to $D_{50\%}$, milling at 200 and 300 rpm for 10, 15 and 20 min reduced the particle size of DC most effectively (Table 4).

The effect of milling on the estimated specific surface area of the material is inversely correlated with particle size. As the particle size of the milled DC decreases, the estimated specific surface area increases with increasing milling time (2 to 20 min) and speed (200 to 300 rpm) (Table 4).

The $D_{50\%}$ of samples milled at 200 rpm for 2 and 5 min was significantly higher than samples milled at 300 rpm for 5, 10 and 15 min, with particle size distribution similar to that obtained for 20 min (Table 4). To produce TC pastes, five DC samples milled first at 200 rpm for 10, 15, and 20 min and 300 rpm for 2 and 20 min were chosen.

The results of the specific milling energy are shown in Figure 4. It is observed that the milling energy increased by 50% as the rotation speed increased from 200 to 300 rpm for the studied milling times. Thus, reaching smaller particle diameters of DC requires higher EM consumption[53,54], when investigating the milling of raw materials for cement production.

The results of the grindability index (GI) of the DC concerning the milling time and the $D_{50\%}$ curves are shown in Figure 4. Grindability measures the predictability of mill performance and the quality of the milled product. The GI tends to decrease with increasing milling time (Figure 4), due to the decreasing particle diameter and increasing estimated specific surface area (Table 4). Furthermore, GI decreases with increasing milling speeds (200 and 300 rpm) due to the increasing estimated specific surface area and the milling energy (SME). Milling for up to 5 min, the speed is the determining parameter in reducing the particle sizes. However, above 10 min, milling does not significantly interfere with DC grindability (Figure 4), indicating reduced variation of the estimated specific surface area and diameter $D_{50\%}$.

3.2. Influence of milling on the reactivity of DC applied in ternary cements

This section presents the results of paste hydration. The ternary cement pastes were identified as TC.i, where i refers to the $D_{50\%}$ of the drilling cuttings used. The heat flow during cement hydration is measured by isothermal calorimetry, as follows: the first stage called the initial period (or pre-induction) is characterized by the rapid increase in the release of heat generated by the dissolution of the C_3S, C_3A, and calcium and alkaline sulfates. It lasts a few minutes, during which the K^+, Na^+, SO_4^{2-}, and Ca^{2+} ions are released into the medium, with an additional contribution of the heat of formation of ettringite from C_3A. In the next stage (induction period), the heat released by the reaction decreases. In this stage, the concentrations of Ca^{2+} and OH^- ions in the liquid phase maximize and, subsequently, decline. The SO_4^{-2} concentration remains constant because as this ion is released by the dissolution of calcium sulfate, it is consumed by the formation of ettringite. At this stage, the hydration of Ca_2SiO_4 is small[54]. In the third stage, called the acceleration period, the reactions speed up, with the precipitation of calcium hydroxide and $Ca_9Si_6O_{18}(OH)_6 \cdot 8(H_2O)$ (C-S-H). The heat flow increases with hydration time and heat release peaks, resulting from the hydration of Ca_3SiO_5, when $Ca_9Si_6O_{18}(OH)_6 \cdot 8(H_2O)$ is formed. Also, Ca_2SiO_4 hydration, calcium hydroxide precipitation, complete dissolution of calcium sulfate and formation of ettringite occur during this period. After 72 hours of hydration, the reaction slows down starting the deceleration period, when the solubilization rate of the anhydrous phases decreases, gradually reducing the rate of heat release[55].

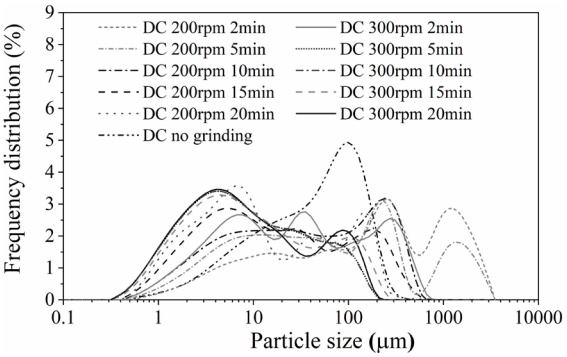

Figure 3. Particle size distribution of the DC after milling.

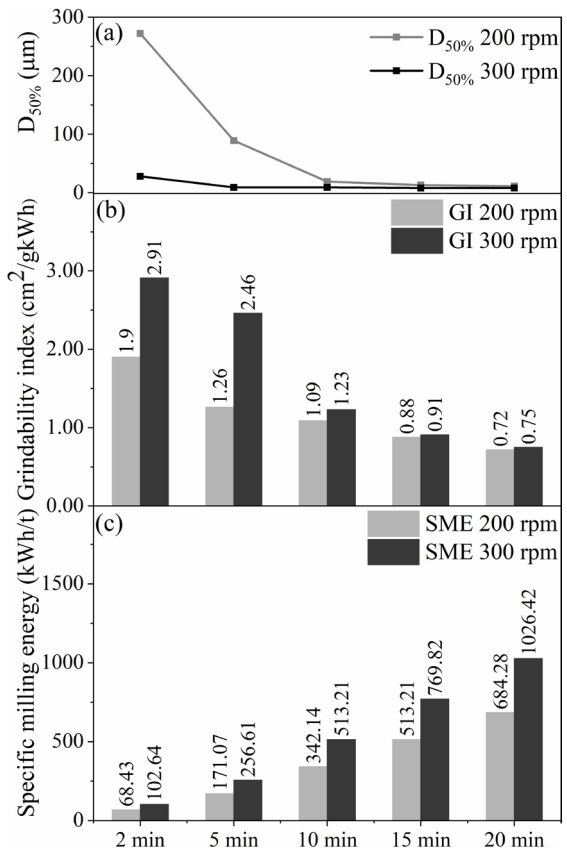

Figure 4. DC diameter $D_{50\%}$ (a), grindability index (b), and specific milling energy (c) in relation to milling time.

Data on the rate of heat released can be used to assess the reactivity of cement and monitor possible production variations[56].

The heat flow curves for the reference and TC samples with added DC of different particle sizes during the first 72 hours are shown in Figure 5. The results of the isothermal calorimetry parameters for pastes are shown in Table 5.

Regarding the TC pastes, the added DC accelerated the hydration kinetics, as shown by the shortening of the induction period, in addition to the increasing heat flow in the induction and acceleration periods (Figure 5 and Table 5). This fact can be explained by the effect of dilution, change in particle packing, and heterogeneous nucleation of the cementitious system[56]. DC accelerated hydration kinetics in the first hours (up to about 8 h) compared to REF.Q and REF.CP pastes, shortening the induction period by up to 3 h and 21 min and 2 h and 55 min, respectively. The end of the induction period is associated with a rapid increase in the formation of $Ca_9Si_6O_{18}(OH)_6.8(H_2O)$ and calcium hydroxide (portlandite)[57]. It is noteworthy that the heat flow at the beginning of the acceleration period was higher for the TC pastes compared to the reference pastes (Figure 5), behavior attributed to the filler effect[55,58]. Similarly[59] also observed $Ca_9Si_6O_{18}(OH)_6.8(H_2O)$ nucleation in different compositions containing SCM. In this context, the results presented suggest that TC pastes may present $Ca_9Si_6O_{18}(OH)_6.8(H_2O)$ nucleation around the DC particles, unlike the REF.Q and REF.PC pastes. This is due to the influence of reduced particle size ($D_{50\%}$) and increased estimated specific surface area since the same mixing energy was applied to the samples.

During the deceleration period, the duration of the hydration reactions was similar for the TC and REF.PC pastes and shorter for the REF.Q paste (Table 5).

The results indicate that as the diameter $D_{50\%}$ of the DC decreases, the hydration reaction of the ternary pastes is accelerated, increasing the reaction rate during the acceleration period and the maximum heat flow (Table 5). This behavior is attributed to the filler effect in studies with cement[58] and pastes containing zeolites[16].

Also, the TC pastes present similar dissolution times (initial times), although the heat flow is minimal for the REF.Q paste (Figure 6). Likewise, the initial and maximum heat flow are higher for the TC samples compared to the reference pastes (Figure 6), as also observed in pastes with kaolinitic clays[60].

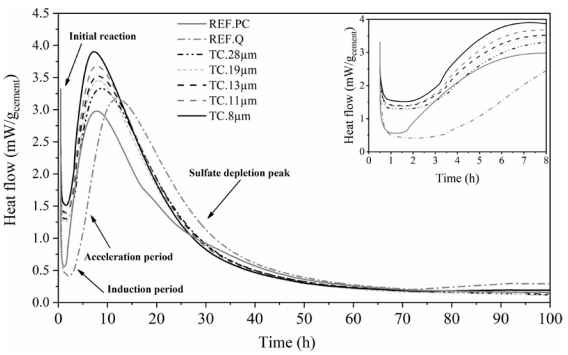

Figure 5. Heat flow in the first 72 hours of cement hydration (20 °C).

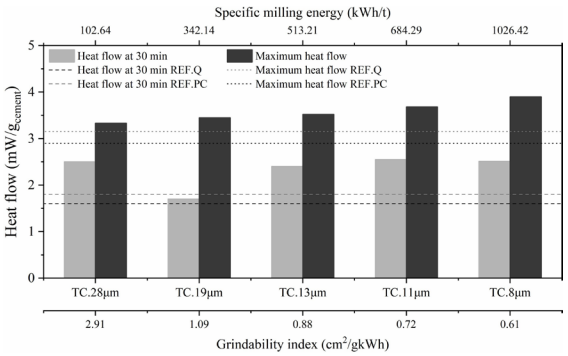

Figure 6. Initial (30 min) and maximum heat flow of ternary cement (TC) in relation to diameter ($D_{50\%}$), milling energy, and grindability index (GI).

Table 5. Hydration parameters of ternary and reference cement pastes obtained by isothermal calorimetry.

Parameters	REF.PC	REF.Q	TC.28µm	TC.19µm	TC.13µm	TC.11µm	TC.8µm
Heat flow at 30 min ($mW.g^{-1}_{cement}$)	1.37	1.54	2.50	1.70	2.40	2.55	2.51
Initial set (h)	1.78	5.9	3.77	3.58	3.56	3.45	3.31
Final set (h)	7.81	12	8.72	8.08	8.18	7.86	7.25
Duration (h)	6.02	6.11	4.95	4.50	4.62	4.42	3.95
Induction period duration (h)	5.00	5.44	2.08	2.56	1.75	1.58	1.35
Acceleration period duration (h)	2.52	6.07	6.01	4.83	5.79	5.61	5.26
Acceleration period maximum heat flow ($mW.g^{-1}_{cement}$)	2.98	3.17	3.33	3.45	3.52	3.68	3.9
Acceleration period slope ($mW.g^{-1}_{cement}\ h^{-1}$)	0.133	0.274	0.332	0.379	0.385	0.440	0.513
Heat of hydration at 24 h ($J\ g^{-1}_{cement}$)	170.9	182.24	204.2	202.51	212.33	216.79	222.96
Heat of hydration at 48 h ($J\ g^{-1}_{cement}$)	233.59	257.42	264.98	258.27	272.52	275.18	279.12
Heat of hydration at 72 h ($J\ g^{-1}_{cement}$)	256.79	282.2	285.63	277.3	293.69	295.53	299.47

The increased adsorption of Ca^{2+} on the surface of DC particles results in an accelerated dissolution of C_3S and growth/increase of C-S-H[61]. Furthermore, the main hydration peak between 8 and 10 hours after the trial began is attributed to the formation of hydrated calcium silicate, calcium hydroxide and ettringite. Compared to REF.PC, the maximum heat flow of TC increased by 0.73 mW/g_{cement} (23%), attributed to the nucleation effect generated by the smaller diameter particles.

The slope of the acceleration period of the TC pastes shows that the hydration rate is higher for TC compared to REF.CP and REF.Q pastes (Figure 7). The presence of the residue is responsible for the filling and nucleation effect of C-S-H[11,59,62,63]. The TC.8μm indicated the maximum slope of the acceleration period, influenced by the decreasing particle size ($D_{50\%}$) and the increase of the estimated specific surface area (Figure 7). Other authors have also reported that the particle nucleation effect may interfere more strongly with the hydration of aluminates compared to silicates[59].

Figure 8 and Figure 9 show the evolution of the accumulated heat. Compared to the reference pastes, the decreasing particle size of DC in the TC pastes differentiates the curves from the initial minutes of hydration, increasing the heat flow over the 72 hours. The evolution of the accumulated heat after 24, 48 and 72 h of hydration is shown in Figure 9. In the TC pastes, reducing the $D_{50\%}$ of DC increased the total heat accumulated over 72 hours, evidencing its accelerating action on the cement hydration process (Figure 8 and Figure 9). The calorimetry indicated that the formation of Ca_3SiO_5 and $Ca_6(Al(OH)_6)2(SO_4)_326(H_2O)$ in the main hydration peak intensified in the TC pastes compared to the REF.Q pastes. The values in Figure 9 also show that the heat accumulated in 72 hours of hydration increased as the DC particle size decreased, which can be attributed to the dilution effect that increases cement hydration, and to the nucleation effect.

The processing of DC was essential to increase the hydration heat during 24, 48 and 72 hours, but it was even more expressive for the TC.19μm, TC.11μm TC.8μm pastes (Figure 9).

For the mineralogical analysis by DRX/Rietveld, the TC.8μm paste was chosen because it is produced with DC of lower $D_{50\%}$. Figure 10 shows the diffraction data of the REF.PC, REF.Q and TC.8μm pastes produced with DC after 3 and 28 days. The crystalline fractions of the samples consist essentially of calcite, quartz, ettringite, ferrite, portlandite, beta belite, illite and dolomite.

Table 6 shows the results of the phase refinement by the Rietveld method and the application of the content of non-crystalline phases for the REF.PC, REF.Q and TC.8μm pastes at 3 and 28 days. The portlandite and ettringite content of the REF.PC sample increased in the hydration periods of 3 and 28 days (Table 6), as well as the consumption of the anhydrous phases (C_2S, C_3S, C_4AF). The increasing content of non-crystalline phases (ACn) is verified at 28 days. The main non-crystalline phase identified in the quantitative analysis is the $Ca_9Si_6O_{18}(OH)_6 \cdot 8(H_2O)$ gel, which is associated with increasing ACn. According to Mehta and Monteiro[64], this behavior is characteristic of cement types/pastes with high initial strength that forms most of the Ca_3SiO_5 in the first days of hydration.

The mineralogical composition of the TC.8μm paste indicates the consumption of the anhydrous phases of Ca_2SiO_4, $Ca_2(Al\ Fe)O_5$ and Ca_3SiO_5 at the ages of 3 and 28 days, thus showing advancing hydration. Additionally, the contents of the $Ca_6(Al(OH)_6)_2(SO_4)_3.26(H_2O)$ and $Ca_9Si_6O_{18}(OH)_6.8(H_2O)$ phases increase in the REF.PC and TC.8μm pastes (Table 6). Since these phases were also observed in the reference samples (no residue), it can be concluded that the DC used for replacing cement partially does not change the characteristic phases of the pastes.

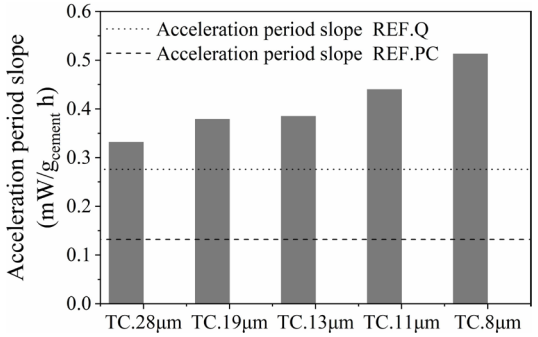

Figure 7. Slope of acceleration period of ternary cement (TC) pastes containing DC.

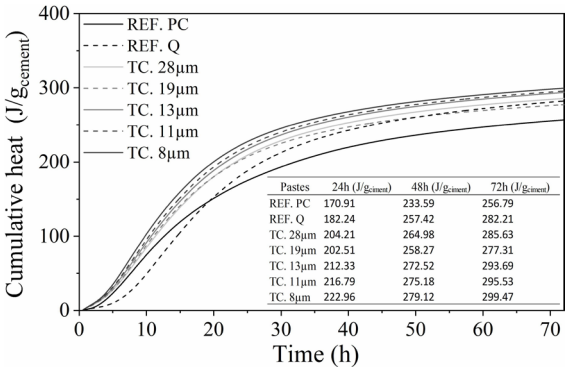

Figure 8. Heat of hydration (cumulative heat) during 72 hours of isothermal calorimetry of cement pastes (20 °C).

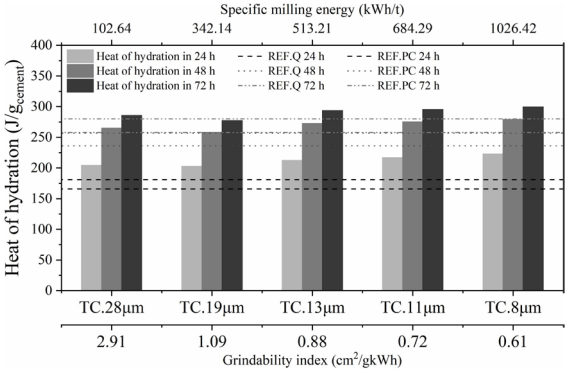

Figure 9. Evolution of hydration heat after 24, 48 and 72 hours in relation to diameter ($D_{50\%}$), milling energy, and grindability index (GI).

The portlandite content increased for TC.8μm and REF.Q pastes at 3 and 28 days (Table 6). The increase in calcium hydroxide content suggests no pozzolanic contribution of DC. In general, $Ca_9Si_6O_{18}(OH)_6 \cdot 8(H_2O)$, $Ca(OH)_2$ and $Ca_6(Al(OH)_6)_2(SO_4)_3.26(H_2O)$ are the main hydrated products of the TC.8μm paste. Additionally, other secondary phases of the precursor raw materials such as $CaCO_3$, SiO_2, $K(Al_4Si_2O_9(OH)_3$, $CaMg(CO_3)_2$ and MgO are identified. The increase in the calcium carbonate content in the REF.PC paste is attributed to the carbonation of the hydrates during sample handling and their contact with the atmosphere during the XRD execution. Although mitigation measures have been guaranteed, exposure of the sample during data collection may promote the interaction of calcium-containing hydrates and CO_2 from the atmosphere, forming additional $CaCO_3$[57].

Previous investigations reported the formation of hemi- and mono-carbo aluminates as hydration products of ternary cements at advanced ages (> 14 days)[65,66]. However, these phases are poorly crystalline, limiting their identification by XRD[67]. It is noteworthy that the absence of phases in the crystalline fraction (sharp peaks) does not mean the absence of carbo aluminates. These phases were previously reported as constituents of the non-crystalline fraction of the cement paste (ACn), being identified by complementary techniques, including thermogravimetric analysis[5,6].

Figure 11 shows the average compressive strength and water absorption of the REF.PC, REF.Q, and TC pastes with added DC after hydrating for 1, 3 and 28 days. DC milling contributed to a decrease (t-test, $p<0.05$) in the water absorption of TC pastes with added DC (Figure 11). The water absorption was higher in the REF pastes and as the particle size of DC decreased so did the water absorption (t-test, $p<0.05$) (Figure 11). The water absorption of the TC 8 mm decreased by approximately 20% compared to the REF CP paste whereas, for the other pastes, it was about 10% and contributed to the closing of the pores. The TC.8 μm paste had the lowest water absorption (t-test, $p < 0.05$) (Figure 11).

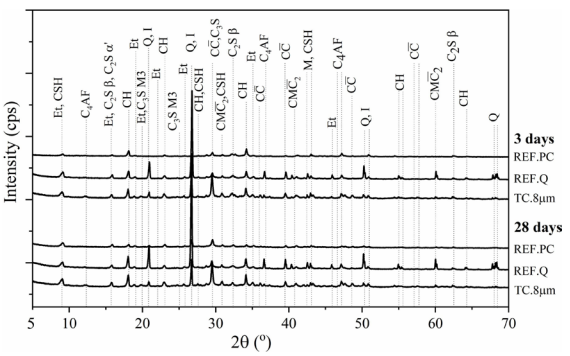

Figure 10. X-ray diffractometry of REF.PC, REF.Q, and TC.8 μm CC: Calcite; Q: Quartz; Et: Ettringite; CH: Portlandite; I: Illite 2M1; C_2S β: Belite β'; CMC_2: Dolomite; M: Periclase; C-S-H: Jennite; C_4AF: Ferrite; C_3S M3: Alite M3, and C_2S α': Belite α'.

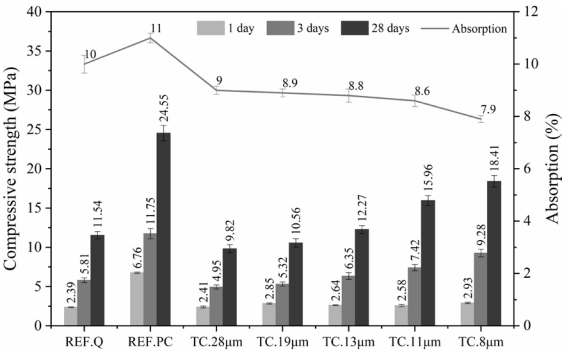

Figure 11. Compressive strength and absorption of REF.PC, REF.Q, and TC pastes with DC.

Table 6. Mineralogical composition of REF.PC, REF.Q and TC.8μm pastes at 3 and 28 days of hydration (wt%).

Composition	Notation	REF.PC		REF.Q		TC.8 μm	
		3 days	28 days	3 days	28 days	3 days	28 days
$CaCO_3$	CC	6.82	13.14	2.94	3.56	10.81	12.10
SiO_2	Q	-	-	33.35	38.74	7.34	6.89
$Ca_6(Al(OH)_6)_2(SO_4)_3\ 26(H_2O)$	Et	8.12	17.25	7.58	6.17	6.61	8.65
$Ca(OH)_2$	CH	12.80	3.90	4.38	5.32	4.42	5.84
$K(Al_4Si_2O_9(OH)_3)$	I	-	-	-	-	3.96	3.73
Ca_2SiO_4	C_2S β	11.37	3.77	-	-	3.70	1.85
$CaMg(CO_3)_2$	CMC_2	-	-	-	-	2.50	3.11
MgO	M	3.70	2.69	1.57	2.04	2.21	1.99
$Ca_9Si_6O_{18}(OH)_6 \cdot 8(H_2O)$	C-S-H	2.57	8.38	2.86	1.67	1.68	2.86
$Ca_2(Al\ Fe)O_5$	C_4AF	2.41	0.00	1.67	1.54	1.67	1.47
Ca_3SiO_5	C_3S M3	2.67	0.00	0.54	0.00	1.05	0.00
Ca_2SiO_4	C_2S α'	0.67	0.00	1.09	0.00	0.84	0.00
ACn (%)		48.87	50.87	41.64	38.76	53.21	51.51
GOF		1.41	2.24	2.39	2.90	1.87	1.94

After 28 days, the average compressive strength of the TC.11μm and TC.8μm pastes are approximately at least 65% and 75% of the REF CP paste, respectively. This result demonstrates the potential application of WM, PG and DC as SCM in ternary cement pastes. As the compressive strength was obtained by replacing approximately 50% of the clinker, less clinker could produce resistance equivalent to that of the PC used.

DC processing consisted of milling only but effectively accelerated the hydration kinetics of ternary cement while stimulating the formation of hydrates responsible for improving the mechanical properties and durability of cementitious materials. The griding also contributed to the filler effect in the TC pastes studied and can be used as an SCM in ternary cement pastes.

4. Conclusions

The provided results and discussions allow the following conclusions:

The milling of DC reduced the particle size by 96% and 70% ($D_{50\%}$) for the studied speeds of 200 and 300 rpm during 2 and 20 min, respectively, thus promoting an increase of milling energy (SME) and decrease of the grindability index (GI). The GI and SME parameters were the most adequate to determine an optimal milling point of the particles as given by the $D_{50\%}$ with varying milling time and speed.

Adding milled DC accelerated the TC hydration kinetics while significantly increasing the reactivity of systems with $D_{50\%}$ diameter smaller than 11 μm. Decreasing the DC particle size reduced the induction period, increased the reaction rate during the acceleration period, as well as increased the maximum heat flow and the slope of the TC heat evolution curve compared to the reference samples. This behavior was attributed to the effect of filling and nucleating of the DC particles added in the TC.

The main hydrated phases of the TC.8μm paste consisted mainly of $Ca_9Si_6O_{18}(OH)_6.8(H_2O)$, $Ca(OH)_2$ and $Ca_6(Al(OH)_6)_2.(SO_4)_3.26(H_2O)$. Also, the other secondary phases of the precursor raw materials are identified, such as $CaCO_3$, SiO_2, $K(Al_4Si_2O_9(OH)_3$, $CaMg(CO_3)_2$ and MgO.

After 28 days, the TC pastes reached at least 70% of the compressive strength of Portland cement paste. Milled DC contributes to the physical and nucleation effect of the TC pastes studied and can be used as an SCM in ternary cement pastes.

5. Acknowledgments

The authors acknowledge the Coordination for the Improvement of Higher Education Personnel (CAPES, Brazil - Grant Nº 451677/2019-1) and the Bahia State Research Support Foundation (FAPESB, Brazil - Grant N° 0397/2018 and 0289/2020) for their financial support. JPG (Proc. N°. 309308/2020–8), and HMCA (Proc. N°. 305280/2021–0) gratefully acknowledge the National Council for Scientific and Technological Development (CNPq, Brazil) for their research grants.

6. References

1. Imbabi MS, Carrigan C, McKenna S. Trends and developments in green cement and concrete technology. Int J Sustain Built Environ. 2012;1(2):194-216.
2. Scrivener KL. Options for the future of cement. Indian Concr J. 2014;88:11-21.
3. Pillai RG, Gettu R, Santhanam M, Rengaraju S, Dhandapani Y, Rathnarajan S, et al. Service life and life cycle assessment of reinforced concrete systems with limestone calcined clay cement (LC3). Cement Concr Res. 2019;118:111-9.
4. De Oliveira JS, Maciel KRD, Dweck J, Andrade HMC, Gonçalves JP. Influence of milling of a reused FCC catalytic waste on the early hydration stages of a special class cement. J Therm Anal Calorim. 2022;147(4):2923-34.
5. Costa ARD, Gonçalves JP. Accelerated carbonation of ternary cements containing waste materials. Constr Build Mater. 2021;302:124159.
6. Costa ARD, Matos SRC, Camarini G, Gonçalves JP. Hydration of sustainable ternary cements containing phosphogypsum. Sustain Mater Technol. 2021;28:e00280.
7. Santos T, Gonçalves JP, Andrade HMC. Partial replacement of cement with granular marble residue: effects on the properties of cement pastes and reduction of CO_2 emission. SN Appl Sci. 2020;2(9):1605.
8. Sánchez Berriel SS, Favier A, Domínguez ER, Machado IS, Heierli U, Scrivener K, et al. Assessing the environmental and economic potential of Limestone Calcined Clay Cement in Cuba. J Clean Prod. 2016;124:361-9.
9. Silva FGS, Fiuza RA Jr, Silva JS, Pinto KW, Andrade HMC, Dweck J, et al. Hydration of the equilibrium catalyst (Ecat) calcium hydroxide system: thermogravimetric study of the formation of main hydrated phases. J Therm Anal Calorim. 2015;120(2):1089-98.
10. Silva FGS, Fiuza RA Jr, Silva JS, De Brito CMSR, Andrade HMC, Gonçalves JP. Consumption of calcium hydroxide and formation of C-S-H in cement pastes: influence of the addition of a spent FCC catalyst (Ecat). J Therm Anal Calorim. 2014;116(1):287-93.
11. Antoni M, Rossen J, Martirena F, Scrivener K. Cement substitution by a combination of metakaolin and limestone. Cement Concr Res. 2012;42(12):1579-89.
12. Avet F, Snellings R, Alujas Diaz A, Haha MB, Scrivener K. Development of a new rapid, relevant and reliable (R3) test method to evaluate the pozzolanic reactivity of calcined kaolinitic clays. Cement Concr Res. 2016;85:1-11.
13. Wan H, Shui Z, Lin Z. Analysis of geometric characteristics of GGBS particles and their influences on cement properties. Cement Concr Res. 2004;34(1):133-7.
14. Snellings R, Mertens G, Elsen J. Supplementary cementitious materials. Rev Mineral Geochem. 2012;74(1):211-78.
15. Zunino F, Scrivener KL. Processing of calcined clays for applications in cementitious materials: the use of grinding aids and particle classification after grinding. In: Martirena-Hernandez J, Alujas-Díaz A, Amador-Hernandez M, editors. Proceedings of the International Conference of Sustainable Production and Use of Cement and Concrete. Cham: Springer; 2020. p. 93-9. (RILEM Book Series; 22).
16. Burris LE, Juenger MCG. Milling as a pretreatment method for increasing the reactivity of natural zeolites for use as supplementary cementitious materials. Cement Concr Compos. 2016;65:163-70.
17. Leonard SA, Stegemann JA. Stabilization/solidification of petroleum drill cuttings. J Hazard Mater. 2010;174(1-3):463-72.
18. Petrobras S.A. Relatório de sustentabilidade 2021. Rio de Janeiro; 2021.
19. Lai H, Lv S, Lai Z, Liu L, Lu Z. Utilization of oil-based mud drilling cuttings wastes from shale gas extraction for cement clinker production. Environ Sci Pollut Res Int. 2020;27(26):33075-84.

20. Al-Dhamri HS, Abdul-Wahab SA, Velis C, Black L. Oil-based mud cutting as an additional raw material in clinker production. J Hazard Mater. 2020;384:121022.
21. Foroutan M, Hassan MM, Desrosiers N, Rupnow T. Evaluation of the reuse and recycling of drill cuttings in concrete applications. Constr Build Mater. 2018;164:400-9.
22. Wang CQ, Lin XY, Wang D, He M, Zhang SL. Utilization of oil-based drilling cuttings pyrolysis residues of shale gas for the preparation of non-autoclaved aerated concrete. Constr Build Mater. 2018;162:359-68.
23. Almabrok MH, McLaughlan RG, Vessalas K. Effect of curing and mixing methods on the compressive strength of mortar containing oil. J Civ Eng Sci Technol. 2015;6(1):6-11.
24. Abousnina R, Manalo A, Ferdous W, Lokuge W, Benabed B, Saif Al-Jabri K. Characteristics, strength development and microstructure of cement mortar containing oil-contaminated sand. Constr Build Mater. 2020;252:119155.
25. Khodadadi M, Moradi L, Dabir B, Nejad FM, Khodaii A. Reuse of drill cuttings in hot mix asphalt mixture: a study on the environmental and structure performance. Constr Build Mater. 2020;256:119453.
26. Shon CS, Estakhri CK. In-situ and laboratory investigation of modified drilling waste materials applied on base-course construction. Int J Pavement Res Technol. 2018;11(3):225-35.
27. Medeiros LC, Câmara APC, Macedo DA, Melo DMA, Melo MAF. Study on the viability of using drill cuttings from the potiguar basin in the production of ceramic products: influence of concentration and firing temperature. Mater Sci Forum. 2014;798-799:224-8.
28. Ravenna MMB, Acchar W, Barros EL No, Silva JB, Silva VM. Study of influence of replacement waste oil well drilling fluid in the standard mass of a ceramic industry in São Gonçalo do Amarante/RN, Brazil. Mater Sci Forum. 2017;881:416-21.
29. Andrade DS, Rego JHS, Morais PC, Rojas MF. Chemical and mechanical characterization of ternary cement pastes containing metakaolin and nanosilica. Constr Build Mater. 2018;159:18-26.
30. Maraghechi H, Avet F, Wong H, Kamyab H, Scrivener K. Performance of Limestone Calcined Clay Cement (LC3) with various kaolinite contents with respect to chloride transport. Mater Struct. 2018;51(5):125.
31. Wongkeo W, Thongsanitgarn P, Poon CS, Chaipanich A. Heat of hydration of cement pastes containing high-volume fly ash and silica fume. J Therm Anal Calorim. 2019;138(3):2065-75.
32. Gettu R, Patel A, Rathi V, Prakasan S, Basavaraj AS, Palaniappan S, et al. Influence of supplementary cementitious materials on the sustainability parameters of cements and concretes in the Indian context. Mater Struct. 2019;52(1):10.
33. Cancio Díaz Y, Sánchez Berriel S, Heierli U, Favier AR, Sánchez Machado IR, Scrivener KL, et al. Limestone calcined clay cement as a low-carbon solution to meet expanding cement demand in emerging economies. Dev Eng. 2017;2:82-91.
34. Medina C, Sáez del Bosque I, Frías M, Sánchez de Rojas M. Design and characterisation of ternary cements containing rice husk ash and fly ash. Constr Build Mater. 2018;187:65-76.
35. El Fami N, Ez-Zaki H, Boukhari A, Diouri A. Rheological behaviour and mechanical properties of Moroccan ternary binder's Portland clinker-fly ash-limestone. Constr Build Mater. 2021;279:122513.
36. Cardoso TC, Matos PR, Py L, Longhi M, Cascudo O, Kirchheim AP. Ternary cements produced with non-calcined clay, limestone, and Portland clinker. J Build Eng. 2022;45:103437.
37. Montani C. XXVII marble and stones in the world report - XXVII Rapporto marmo e pietre nel mondo. Carrara: Aldus Casa Di Edizioni; 2016.
38. Aydin E, Arel HŞ. High-volume marble substitution in cement-paste: towards a better sustainability. J Clean Prod. 2019;38: 117801.
39. Uygunoɨlu T, Topçu IB, Çelik AG. Use of waste marble and recycled aggregates in self-compacting concrete for environmental sustainability. J Clean Prod. 2014;84:691-700.
40. Rashad AM. Potential use of phosphogypsum in alkali-activated fly ash under the effects of elevated temperatures and thermal shock cycles. J Clean Prod. 2015;87:717-25.
41. IAEA: International Atomic Energy Agency. Radiation protection and management of NORM residues in the phosphate industry. Vienna; 2013. (Safety Reports Series; 78).
42. Kong L, Price L, Hasanbeigi A, Liu H, Li J. Potential for reducing paper mill energy use and carbon dioxide emissions through plant-wide energy audits: a case study in China. Appl Energy. 2013;102:1334-42.
43. Damineli BL, John VM, Lagerblad B, Pileggi RG. Viscosity prediction of cement-filler suspensions using interference model: a route for binder efficiency enhancement. Cement Concr Res. 2016;84:8-19.
44. Semiz B. Characteristics of clay-rich raw materials for ceramic applications in Denizli region (Western Anatolia). Appl Clay Sci. 2017;137:83-93.
45. Yu J, Mishra DK, Hu C, Leung CKY, Shah SP. Mechanical, environmental and economic performance of sustainable Grade 45 concrete with ultrahigh-volume Limestone-Calcined Clay (LCC). Resour Conserv Recycling. 2021;175:105846.
46. Sharma M, Bishnoi S, Martirena F, Scrivener K. Limestone calcined clay cement and concrete: A state-of-the-art review. Cement Concr Res. 2021;149:106564.
47. ASTM: American Society for Testing and Materials. ASTM C1679-17: standard practice for measuring hydration kinetics of hydraulic cementitious mixtures using isothermal calorimetry. West Conshohocken: ASTM; 2017.
48. ASTM: American Society for Testing and Materials. ASTM C1702-17: standard test method for measurement of heat of hydration of hydraulic cementitious materials using isothermal conduction calorimetry. West Conshohocken: ASTM; PA 2017.
49. Toby BH, Von Dreele RB. GSAS-II: the genesis of a modern open-source all-purpose crystallography software package. J Appl Cryst. 2013;46(2):544-9.
50. Abu MJ, Mohamed JJ, Ahmad ZA. Synthesis of high purity titanium silicon carbide from elemental powders using arc melting method. Int J Refract Hard Met. 2014;47:86-92.
51. Calligaris GA, da Silva TLT, Ribeiro APB, dos Santos AO, Cardoso LP. On the quantitative phase analysis and amorphous content of triacylglycerols materials by X-ray Rietveld method. Chem Phys Lipids. 2018;212:51-60.
52. Madsen IC, Scarlett NVY, Kern A. Description and survey of methodologies for the determination of amorphous content via X-ray powder diffraction. Z Kristallogr. 2011;226(12):944-55.
53. Ghalandari V, Esmaeilpour M, Payvar N, Toufiq Reza M. A case study on energy and exergy analyses for an industrial-scale vertical roller mill assisted grinding in cement plant. Adv Powder Technol. 2021;32(2):480-91.
54. Pradhan P, Mahajani SM, Arora A. Pilot scale production of fuel pellets from waste biomass leaves: effect of milling size on pelletization process and pellet quality. Fuel. 2021;285:119145.
55. Bullard JW, Jennings HM, Livingston RA, Nonat A, Scherer GW, Schweitzer JS, et al. Mechanisms of cement hydration. Cement Concr Res. 2011;41(12):1208-23.
56. Lawrence P, Cyr M, Ringot E. Mineral admixtures in mortars: effect of inert materials on short-term hydration. Cement Concr Res. 2003;33(12):1939-47.
57. Scrivener KL, Juilland P, Monteiro PJM. Advances in understanding hydration of Portland cement. Cement Concr Res. 2015;78:38-56.
58. Schöler A, Lothenbach B, Winnefeld F, Haha MB, Zajac M, Ludwig HM. Early hydration of SCM-blended Portland cements: a pore solution and isothermal calorimetry study. Cement Concr Res. 2017;93:71-82.

59. Berodier E, Scrivener K. Understanding the filler effect on the nucleation and growth of C-S-H. C. J Am Ceram Soc. 2014;97(12):3764-73.
60. Alujas A, Fernández R, Quintana R, Scrivener KL, Martirena F. Pozzolanic reactivity of low grade kaolinitic clays: influence of calcination temperature and impact of calcination products on OPC hydration. Appl Clay Sci. 2015;108:94-101.
61. Snellings R, Mertens G, Cizer Ö, Elsen J. Early age hydration and pozzolanic reaction in natural zeolite blended cements: reaction kinetics and products by in situ synchrotron X-ray powder. Cement Concr Res. 2010;40(12):1704-13.
62. Lothenbach B, Scrivener K, Hooton RD. Supplementary cementitious materials. Cement Concr Res. 2011;41(12): 1244-56.
63. Oey T, Kumar A, Bullard JW, Neithalath N, Sant G. The filler effect: the influence of filler content and surface area on cementitious reaction rates. J Am Ceram Soc. 2013;96(6):1978-90.
64. Mehta PK, Monteiro PJ. Concreto: microestrutura, propriedades e materiais. 3ª ed. São Paulo: IBRACON; 2008. (vol. 3).
65. Avet F, Scrivener K. Investigation of the calcined kaolinite content on the hydration of Limestone Calcined Clay Cement (LC3). Cement Concr Res. 2018;107:124-35.
66. Zunino F, Scrivener K. Microstructural developments of limestone calcined clay cement (LC3) pastes after long-term (3 years) hydration. Cement Concr Res. 2022;153:106693.
67. Krishnan S, Bishnoi S. Understanding the hydration of dolomite in cementitious systems with reactive aluminosilicates such as calcined clay. Cement Concr Res. 2018;108:116-28.